Clim. Past Discuss., 9, 1803–1839, 2013
www.clim-past-discuss.net/9/1803/2013/
doi:10.5194/cpd-9-1803-2013

Climate of the Past Discussions
Open Access

A regional climate palaeosimulation for Europe in the period 1500–1990 – Part 1: Model validation

J. J. Gómez-Navarro[1], **J. P. Montávez**[2], **S. Wagner**[1], **and E. Zorita**[1]

[1]Institute for Coastal Research, Helmholtz-Zentrum Geesthacht, Geesthacht, Germany
[2]Department of Physics, Regional Campus of International Excellence "Campus Mare Nostrum", University of Murcia, Murcia, Spain

Received: 14 March 2013 – Accepted: 28 March 2013 – Published: 5 April 2013

Correspondence to: J. J. Gómez Navarro (juan.gomez-navarro@hzg.de)

Published by Copernicus Publications on behalf of the European Geosciences Union.

Abstract

We present and analyse a high-resolution regional climate palaeosimulation encompassing the European region for the period 1500–1990. We use the regional model MM5 coupled to the global model ECHO-G. Both models were driven by reconstructions of three external factors: greenhouse gas concentrations, Total Solar Irradiance and volcanic activity. The simulation has been assessed in a recent period by comparing the model results with the Climate Research Unit (CRU) database. The results show that although the regional model is tightly driven by the boundary conditions, it is able to improve the reliability of the simulations, narrowing the differences to the observations, especially in areas of complex topography. Additionally, the evolution of the spatial distributions of temperature and precipitation through the last five centuries has been analysed. The mean values of temperature reflects the influence of the external forcings but, contrary to the results obtained under climate change scenario conditions, we found that higher-order momenta of the probability distribution of seasonal temperature and precipitation are hardly affected by changes in the external forcings

1 Introduction

Although the physical mechanisms conductive to global higher temperatures accompanying an increase of atmospheric concentrations of anthropogenic greenhouse gases are well understood, the magnitude of future projections of climate change are still burdened with large uncertainties. This is even more pronounced at regional scales, where additional processes and feedbacks may modulate the climate response to external forcings (Christensen. et al., 2007), especially over extratropical regions, where the internal variability of the atmosphere and the ocean may mask the impact/influence of changes of external climate forcings.

The comparative analysis of proxy-based climate reconstructions and climate simulations was proposed as a means to reduce the spread in the uncertainties of climate

CPD
9, 1803–1839, 2013

sensitivity (González-Rouco et al., 2009; Gómez-Navarro et al., 2011; Zorita et al., 2010, among others). This type of comparative analysis can furthermore provide useful information about the amplitude of externally unforced climate variations, the processes involved therein and about the skill of climate models in simulating regional climate changes. The latter goal seems particularly important because the estimation of climate change impacts and possible adaptation measures depend on the level of certainty that can be placed on simulated regional climate change projections. However, one important remaining factor refers to the discrimination and quantification of different sources of error, ranging from uncertainties in external forcings to sensitivity and physical parameterizations of global and regional climate models.

The direct comparison between individual proxy records and simulations is hampered by the limited resolution of global climate models, presently about 200–300 km at mid-latitudes. For comprehensive AOGCMs used in paleoclimatological studies, this resolution might be up to 400 km. Regional characteristics related to a detailed representation of topography and coastlines might cause deviations between simulations and proxy series, which would not be per se indicative of a serious intrinsic deficiency of the global climate model. Although computationally expensive, regional models are a useful tool to better simulate regional climate changes. Driven at the boundaries of a limited domain by the output of global models, they can represent much more realistically, thanks to their high spatial horizontal resolution of about 20 to 50 km and a more realistic representation of the physical processes, i.e. parameterizations at local scales, all those regional characteristics that can be important to interpret a particular proxy record. In some instances they can also produce a more realistic frequency or intensity of regional synoptic circulation patterns, so that the imprint of a large-scale climate change signal on the local climate is also better represented.

In this study we focus on the evolution of the climate of the European region during the last five centuries. This period was subject to an intense analysis based on empirical climate reconstructions (Luterbacher et al., 2004; Pauling et al., 2006). Those reconstructions are based on a variety of different sources, e.g. related to a very rich

CPD
9, 1803–1839, 2013

web of recorded historical evidence, very long instrumental and early instrumental climate series, tree-rings, lake sediments, etc.) and thus offer a suitable basis for comparisons with climate model simulations. Additionally, a few very long, almost 400 hundred year-long instrumental temperature series, such as the Central England temperature record, are available. All these sources were combined into gridded reconstructions of monthly (or seasonal for early periods) near-surface air temperature (SAT) and precipitation, which are particularly useful for comparisons with coarse-resolution simulations (Luterbacher et al., 2004; Pauling et al., 2006). Although uncertainties in the instrumental and early instrumental records cannot be ignored, particularly in their early part, they are probably more closely ground-truthed than other indirect indicators of temperature. This is particularly important in situations when disagreements between model simulations and reconstructions purely based on natural proxies can not be completely resolved.

As previously mentioned, comparisons with reconstructions, as well as the assessment of the role of internal versus externally-forced variability at high regional scale, requires high-resolution simulations over long periods of time, demanding high computational costs. Consequently, only few high-resolution climate simulations are available over this area. Gómez-Navarro et al. (2011) studied the evolution of the climate through a millennial simulation over the Iberian Peninsula, by comparing the simulation output with available climate reconstructions, and used different simulations sharing the same external forcings to analyse the role of internal variability (Gómez-Navarro et al., 2012). Schimanke et al. (2012) employed a regional climate model and a regional ocean model to study the evolution of climate in the Baltic Sea region during the last millennium and perform sensibility studies.

The added value of regional climate models is normally established by estimating the degree of agreement between the model results and a set of observations. This approach can be misleading to model developers because the mismatch between simulations and observations includes different types of errors. A comparison does not allow to establish whether the added value provided by the regional model is just due

CPD
9, 1803–1839, 2013

to the higher resolution, or based on improvements within the model in the simulation of the underlying physical processes (Kanamitsu and DeHann, 2011). However, from the point of view of the final users of climate simulations, this distinction might be less important. The output of global and regional models is viewed as a source of potentially useful data, regardless of the real causes of the model deficiencies. This is the point of view that we adopt in this manuscript.

An important aspect in the context of real improvements, besides the mean climatic differences between models and observations, relates to the second moments, i.e. climate variability. In this context the study of Murphy (1999) argue that statistical applications, i.e. interpolation of GCM results onto higher resolved topography taking into account lapse rates, considerably improves model biases. Therefore an important question is whether regional climate models are also improving the variance and bandwidth of climate variables at regional scales related to their probability density functions. These metric/comparisons will also be assessed/carried out within this study.

Another aspect of the added value discussed by Kanamitsu and DeHann (2011) is the importance of its spatial distribution. These authors demonstrate that the added value is not spatially homogeneous, but rather tends to be more noticeable over or close to areas of complex orography. Thus, the geographical distribution of skill can be a piece of useful information for the user. This issue has been demonstrated in many other regional studies. For instance, Prömmel et al. (2009) illustrated the added value, with respect to the driving data, of a high-resolution hindcast simulation over the Alpine region, and demonstrated its distribution over complex areas. Thus, in this study we set out to identify areas where the added value of the regional model is more noticeable, as well as identifying areas where the use of coarse-resolution climate simulations, without the use of any downscaling technique, is a reasonable choice.

The objective of the present study is to identify the added value of a high-resolution climate paleosimulations for Europe with respect to state-of-the-art GCMs, as well as to show the skill and drawbacks of the MM5-ECHO-G set-up to reproduce a realistic climate for the last centuries. The comparison between the model simulation with

CPD
9, 1803–1839, 2013

currently available climate reconstructions for Europe will be performed in a follow-up paper. After presenting the technical details of the climate simulations along with a short summary of the observational data set employed as reference in this study, we present in Sect. 3 a validation of the climate simulations for the present-day climate. Section 4 analyses the evolution of Probability Distribution Functions in different key periods of time within the simulation. Finally, the paper is closed with the main conclusions and outlook implications of this study.

2 Data and simulations details

For this study we performed a 490 yr long regional simulation of the European climate over the period 1501–1990 AD. The RCM employed is a climate version of the meteorological model MM5 driven at its domain boundaries by the AOGCM ECHO-G (the model configuration will be hereafter referred to as MM5-ECHO-G). Both models were driven by the same external forcings that will be further explained in greater detail below.

The ECHO-G global model driving the RCM consists of the spectral atmospheric model ECHAM4 coupled to the ocean model HOPE-G (Legutke and Voss, 1999). The model ECHAM4 was used with a horizontal resolution T30 ($\sim 3.75^{\circ} \times 3.75^{\circ}$) and 19 vertical levels. The horizontal resolution of the ocean model is approximately $2.8^{\circ} \times 2.8^{\circ}$, with a grid refinement in the tropical regions and 20 vertical levels to allow for a better representation of ENSO and related phenomena. A flux adjustment between the atmosphere and ocean submodels, constant in time and with vanishing spatial average, was applied to avoid climate drift.

The model was driven by estimations of three independent sources of external forcings: greenhouse gas (GHGs) concentrations in the atmosphere, long-term variations in total solar irradiance (TSI) and an estimation of the global radiative forcing of stratospheric volcanic aerosols. The last two effects are included through the introduction of

CPD
9, 1803–1839, 2013

variations in an effective solar constant. A full description of this simulation and their external forcings can be found in (Zorita et al., 2004, 2005, and references herein).

The forcings employed in the simulations were taken from the Crowley (2000) reconstructions, and their evolution is depicted in Fig. 1. The orange line represents the reconstruction employed for the variability of the TSI. It has been scaled to represent a difference of 0.3 % (around 4 $W m^{-2}$) between the TSI values of the Maunder Minimum and present day values. It is noteworthy that more recent studies in the context of long-term variations in solar activity suggest a considerably larger bandwidth of potential amplitudes. For instance, the Krivova et al. (2007) reconstruction scaling reflects an amplitude of 1.3 $W m^{-2}$, whereas Shapiro et al. (2011) suggests even larger values around 6 $W m^{-2}$. Currently there exists an ongoing debate regarding this particular issue (Gray et al., 2011), and thus using the Crowley (2000) reconstruction for TSI represents reasonable choice in the center of current scalings.

The simulations also consider the effect of volcanic activity through the estimation of the net effect in the radiative balance, shown in the black line of Fig. 1. The sum of changes in long-term TSI and volcanic eruptions is integrated into an effective solar constant, which is implemented in the model to take into account both sources of external forcings. The time series of the effective TSI indicates a number of maxima and minima, of which two minima around 1700 and 1810 stand out. These periods refer to solar anomalous periods related to the Maunder and Dalton Miminum no or only very few sunspots in the solar disc. Another important characteristic of these periods is the simultaneous increase in volcanic activity.

The black, green and grey lines of Fig. 1 represent the evolution of carbon dioxide, nitrous oxide and methane, respectively. GHG concentrations show relatively constant values until 1850 AD, when the industrial period begins. Afterwards, the GHG concentrations increase globally until the end of the simulated period in 1990. In a following chapter it will be discussed how this increase is accompanied by an increase in SAT. Other external forcings related to tropospheric aerosols, changes in land-use and

CPD
9, 1803–1839, 2013

astronomical parameters, were not considered. In order to avoid physical inconsistencies both models, GCM and RCM, were driven by identical external forcings.

The regional climate model used for the present study is the climate version of the Fifth-Generation Pennsylvania-State University-National Center for Atmospheric Research Mesoscale Model (Dudhia, 1993; Grell et al., 1994; Gómez-Navarro et al., 2011; Jerez et al., 2012). Two two-way nested domains were employed in the simulation with a spatial resolution of 135 km and 45 km, respectively. Figure 2 depicts the inner domain, with the actual topography implemented in the model. The present study focuses on this domain. The atmosphere is represented by 24σ levels in the vertical, with the top level located at 100 hPa. The boundary conditions of the model ECHO-G are assimilated into the RCM through a blending area of five grid points at the fringes of the outer domain. These areas are not reliable in general and are excluded from the analysis hereafter.

The configuration of the model physics in the RCM was chosen to minimise the computational cost. This cost criterion was selected because none of the tested configurations provides an optimal performance for different kinds of synoptic events and regions (Fernández et al., 2007; Jerez et al., 2012). The physical options implemented are as follows: Grell cumulus parametrisation (Grell, 1993), Simple Ice for microphysics (Dudhia, 1989), RRTM radiation scheme (Mlawer et al., 1997) and MRF for boundary layer (Hong and Pan, 1996). The Noah Land-Surface model (Chen and Dudhia, 2001a,b) was used, because it simulates more accurately the climate in dry areas, especially in summer over most of the IP (Jerez et al., 2010). Boundary conditions are updated at the boundaries of the regional model every 12 h.

To assess the skill of the model MM5-ECHO-G in reproducing the climate in a recent past period, we compare the seasonal mean values of SAT and precipitation with the monthly data set developed by the Climate Research Unit (CRU) at the University of East Anglia (Harris et al., 2012). The CRU (dataset version CRU TS3.00) is a gridded product that extends over the global land surface with a spatial resolution of 0.5° × 0.5° and includes several climatic variables for the period 1901–2005 AD. However, for the

CPD
9, 1803–1839, 2013

comparison purposes in this analysis only temperature and precipitation series up to 1990 are considered. The data were interpolated onto the regional model grid to provide a better basis for comparisons. Due to missing information over oceanic parts in the CRU data set, only land points areas are considered for the comparison.

3 Reproducing the present climate

We have assessed the model skill in reproducing a realistic climate to highlight the improvement of the regional climate simulation over the global model, but also to identify possible important deficiencies. This assessment has focused on the comparison of several climate parameters in the simulation and in the CRU observational datasets in a reference period. Some statistics of the seasonal series of SAT and precipitation are analysed in Sect. 3.1, whereas the analysis of Probability Distribution Functions (PDFs) is discussed in Sect. 3.2.

3.1 Climatologies during 20th century

We have first assessed the skill of the coupled model MM5-ECHO-G to reproduce the observed climate in the period 1960–1990 (hereafter referred as the reference period). We specifically focus on seasonal mean values and variability of SAT and precipitation. For this purpose we have used the CRU data base (Harris et al., 2012).

Figure 3 depicts the time-averaged SAT in winter (left panels) and summer (right panels) for the reference period in the model (top panels), in the observations (middle panels) and their difference (bottom panels). The significance of these differences has been tested though a two-tailed t test, as indicated with a small black circles in the maps. In winter, the model describes the general spatial pattern relatively well, with the coldest areas in the northeastern part of the domain and the warmest in North Africa. Some deviations appear nevertheless more clearly when looking at the difference pattern. Although the model accurately simulates the temperature in the areas close to

CPD
9, 1803–1839, 2013

the Mediterranean sea, with an average warm bias of 0.3 K in the areas south of 45° N, and few areas with significant differences over the Iberian Peninsula, it is clearly too warm in northern Europe (the averaged warm bias is 2.8 K for the areas north of 45° N, and it is larger than 5 K in some areas). This picture is inverted in summer when the model is too cold. Again, the model seems to simulate the general pattern relatively well (in particular it is able to capture the main mountain systems), but a marked difference in northern and southern Europe is clear. In this season the model is too cold, more remarkably in areas near the Mediterranean sea (the averaged cold bias over the Iberian Peninsula is −3.9 K). Although significant, these warm/cold bias are within the ranges simulated, for the present climate, by other in the state-of-the art RCMs employed for climate change projections in Europe (Christensen. et al., 2007).

Figure 4 depicts the similar information than Fig. 3 for precipitation. Wettest areas in winter are near the western coasts and in the main mountain regions, as corresponds to a circulation dominated by the westerly moist flow. The model is able to capture this behaviour to a large extent. However, some differences appear in the difference map (bottom row). In winter there is a clear bipolar behaviour: the model overestimates the precipitation in northern Europe, but underestimates it in the Mediterranean area. The same bipolar behaviour, but inverted, is found in summer, although in this case the bias is smaller and in many areas it is not statistically significant. In this season, the largest precipitations are related to the orography (see Fig. 2), and the resolution employed in the simulation is able to reproduce this behaviour to a large extent (the spatial correlation between model and observations is 0.71). However, important bias still remain in these areas, especially over the Alps and the Pyrenees. These differences can be attributed to model or observation deficiencies. On the models side, it has to be borne in mind that the 45 km resolution of the model can not capture high-resolution orographic features such as valleys, which play an important role in these areas. Regarding the gridded observations, spatial interpolation of observations to create gridded products is especially difficult over mountainous areas, where spatial correlations may be low (Osborn and Hulme, 1997).

CPD
9, 1803–1839, 2013

We have investigated the reasons for the warm and wet bias in Northern Europe. The warm bias in winter is already present in the stand-alone ECHO-G simulation, with the notably difference of a strong cold bias in the most northeastern part of the domain (not shown). In ECHO-G the warm bias is even larger near the Mediterranean, pointing to a improvement in this area due to the higher resolution of the RCM. This warm bias in northern Europe seems caused by an overestimation of the strength of the zonal circulation, which advects too much warm and moist air from the Atlantic sea. This overestimation is due to a too intense pressure gradient simulated by ECHO-G, as can be appreciated in Fig. 5, where the mean sea level pressure (MSLP) in the reference period for the NCEP reanalysis (Kalnay et al., 1996) and ECHO-G is presented. The flow associated with this pressure gradient is introduced into the RCM through the boundaries of the domain, warming the area in winter. The anomalous flow of warm moist air from the ocean also explains the larger precipitation amounts in this season in northern Europe.

The cold bias in summer is also present in the ECHO-G simulation, with the exception of the main mountain systems. Here, the bias is smaller since the GCM is not able to represent the mountain ranges due to its coarse resolution (not shown). The RCM is still able to reduce the bias over these mountains, but it cannot be completely corrected. Comparing Figs. 3 and 4, the cold bias in summer near the Mediterranean is linked to too wet conditions. A possible explanation may involve a too extensive cloud cover and precipitation in summer, thus reducing the incoming solar radiation and cooling this area relative to the observations. This hypothesis, though plausible, is hard to test due to the lack of reliable observations of the cloud fraction over this area for the reference period.

We have also evaluated the variability of the model and its spatial structure against the observations in the reference period. Figure 6 shows the SAT variability (standard deviation) of the seasonal means in winter and summer for the model (top panels), as recorded in the observations (middle panels) and their ratio (bottom panels). As before, the significance of these differences has been tested, in this case with a two-tailed

CPD
9, 1803–1839, 2013

F test, and is indicated with a small black circles in the maps. In winter, the variability in both the model and the observations is larger than in summer, more notably in the northern areas. The model underestimates the winter variability in general, although only in some areas, such as central Europe, the simulated variability is up to a third of the observed. Despite this general underestimation of the variability of seasonal SAT series in the model, the spatial structure is very similar (spatial correlation 0.84), with a clear northwestern-southeastern gradient. Similarly, the model is generally less variable in summer, with the largest deviations in northeastern Europe, where they become significant. There are two clear areas, in the Northwest of the Iberian Peninsula and the West of Scandinavia, where the model develops an excess of variability, although it is not statistically significant. Figure 7 depicts the same information for precipitation. Usually, precipitation variability is linearly related to its mean value, and this explains why the ratio patterns in this figure are similar to those of the difference in the mean (Fig. 4). Nevertheless, this pattern is patchy, and no clear pattern of underestimation of overestimation of precipitation variability, beyond the aforementioned link between precipitation variability and amount, can be identified.

The next step was to analyse the simulated and observed long-term trends. For this statistics we have considered a longer period, 1900–1990, which allows to evaluate the simulated warming trend during the 20th century and compare it with the observations. Figure 8 represents the trend in the SAT series for winter and summer during this period (top panels) and the CRU database (bottom panels). Significance of these trends have been tested with the non-parametric Mann–Kendall test (assuming that series are serially uncorrelated) and indicated with black circles in the figure. Compared with the observations, the model clearly overestimates the final warming trend, especially in winter and over the northern areas. The CRU database exhibit a negative trend around the Baltic sea, which is absent in the simulations. Although these trends are not significant due to the large variability in these areas (see Fig. 6) there are two physical possible explanations for this difference behaviour. On the one hand, these simulations do not include the forcing due to anthropogenic tropospheric aerosols. Thus, they do

CPD
9, 1803–1839, 2013

not take into account the increase in aerosol concentrations that has taken place during the last part of the simulation. This forcing.albeit with large uncertainties, is believed to cause a net cooling. On the other hand, a great part of this overestimation of the warming trend in winter can be attributed to the increase of zonal circulation produced by the driving model during this period. This can be clearly appreciated in the NAO index simulated by de model and depicted in Fig. 1. This anomalous increase in the zonal circulation that describes the strengthening of NAO during the last century of the simulation, may explain part of the warming trend in winter in the coldest areas of Europe. It has to be noted that the long-term evolution of NAO, and thus other related variables such as especially precipitation, is to a great extent driven by internal variability (Gómez-Navarro et al., 2012), and thus agreement between observations and simulations can not be expected even if the model were perfect. Similarly, Fig. 9 represents the trends simulated and observed for precipitation during the 20th century. Although the observation pattern is patchy, the model exhibits a clear bipolar structure in winter, with larger precipitation in Northern Europe and lower in the South. This bipolar structure is again compatible with the hypothesis of an intensification of the zonal circulation in the last part of the last century that is not present in the observations. Whether or not the trend in the circulation is caused by the increase in the radiative forcing over the 20th century is unclear, since the simulated NAO response in scenario simulations is still model dependent (Miller et al., 2006), and possibly resolution dependent along model versions of the same basic model (Bladé et al., 2012).

Summarizing this section, the coupled model MM5-ECHO-G is able to reproduce many aspects of the present climate in Europe. Some biases compared to the CRU data base can be found in the reference period, although they are within the range of of other biases simulated by current state-of-the art RCMs employed in climate change projections. In particular, winters tend to be too warm and wet, and summers too cold. This underestimation of the amplitude of annual cycle seems to be related to an overestimation of the zonal flow in the GCM, as well as to an overestimation of the precipitation amount, mostly near the Mediterranean sea in summer. However, the analysis

CPD
9, 1803–1839, 2013

of the trends during the 20th century shows that the overestimation of zonal circulation has been especially noticeable in the last part of the simulation (when the forcings are larger), which is the period employed here as validation. Thus, the size of these biases can be expected to be equal or even smaller during the simulated past. Finally, it is important to note that the model tends to underestimate the interannual SAT variability compared to observations (see Fig. 6), and this can bear some relevance when comparing the variability of long-term series in the model and in proxy-based reconstructions.

3.2 Probability distribution functions

In this section we analyse the Probability Distribution Functions (PFDs) of seasonal series of SAT and precipitation over different areas, trying to emphasize the added value of the regional simulation, as well as identifying where it is especially noticeable.

Figure 10 shows the PDFs of the seasonal series of SAT for winter and summer during the 20th century as simulated by the GCM, the RCM and in the CRU dataset. For this calculation, a longer period (1900–1990) has been considered to increase the sample size, given that we deal with seasonal series, and thus to improve the representativeness of the PDFs. Each PDF have been calculated independently for every grid point, and then spatially-averaged. In order to avoid averages over too large areas, which would dilute the added value of the RCM model at regional scales, nine areas have been selected according to geographical guidelines (shown in Fig. 2). Comparing the MM5 results with the observations (lines blue and red, respectively), it is again apparent that the model tends to overestimate winter temperature, especially in central and eastern Europe. The opposite behaviour is found in summer, leading to the underestimation of the annual cycle discussed above. The added value of the regional simulations can be better appreciated by comparing GCM and RCM results (lines blue and green, respectively). Although the mean temperature in the regional model is largely determined by the GCM, in most areas the regional model tends to narrow differences from the observations, especially when the bias is large, as in the

CPD
9, 1803–1839, 2013

Balkan Peninsula in winter or Scandinavia in summer. There are, however, some areas where the bias introduced by the regional model is less significant, as in Central Europe, where the differences between both models are small. This lack of added value can be explained by the flat orography of these regions, which renders the use of high resolution simulations not so important. Finally, it is important to note that in some areas the bias in the regional simulation increases, as in Turkey or eastern Europe in summer. There is, however, no satisfactory explanation for this unexpected behaviour. One aspect where the RCM more clearly demonstrates its added value with respect to the coarse-resolution GCM is its capability to reproduce the shapes of the observed PDFs. In areas of complex topography, like the Iberian Peninsula or the Alps, the GCM is not capable of reproducing a realistic PDF (bimodal in the first case and especially flat and skew in the second), but the RCM, although with an spatially average value tightly driven by the GCM, is able to reproduce the main features of these characteristic PDFs. However, it is worth noting that the shape of these PDFs is not determined by the local variability, but by the spatial variability of temperature within each region. Thus, the bimodality in the Iberian Peninsula in summer, for instance, is not due to the interannual variability, but to a bipolar behaviour of mean temperature in different parts of this area. This is apparent when considering temperature deviations from the long-term mean. When PDFs are calculated from these anomalies series (figures not shown for the sake of brevity) they do not show bimodality or skewness, and the range of the PDF generated by both models match pretty well the observations.

Figure 11 represents the PDFs for the seasonal precipitation in the same nine areas as before. In winter, the overestimation of zonal circulation prompts ECHO-G to overestimate precipitation regimes relative to the observations. The regional model is able to partly correct these biases, reducing the overestimation of precipitation and narrowing differences with the observations, specially in areas of complex topography such like Turkey, the Alps or the Iberian Peninsula. However, in areas where precipitation is strongly dominated by the zonal flow, such as Scandinavia, or where the higher resolution of the RCM does not makes a big difference due to their flat orography, like

CPD
9, 1803–1839, 2013

Eastern and Central Europe, MM5 develops a similar climatology as the driving model, resulting in an overestimation of precipitation also in the regional model. In summer, both models reproduce the strong skewness of precipitation PDF over dry areas, such as Turkey, The Balkans or the Iberian Peninsula, although the regional model displays a better performance in seasons with mean precipitation below 20 mm month^{-1}. In the rest of the areas, the MM5 climatology is closer to observations, more noticeably in the right tail of the distribution, where ECHO-G underestimates precipitation. As before, in Central Europe there is no clear gain from the high resolution simulation.

4 Evolution of PDFs through the simulation

All climate change projections with state-of-the-art climate models produce a warming trend during the 21st century, and in some of them the warming trend is accompanied by an intensification of the some type of extreme episodes under greenhouse-forced conditions (Christensen. et al., 2007). A relevant question that can be addressed with this simulation is whether changes in the probability distribution can be identified in palaeoclimate simulations.

With this purpose, we have calculated the PDFs of the seasonal series of SAT and precipitation in different periods to analyse their changes over time. We have selected a reference period in the last part of the simulation when the anthropogenic forcing is more noticeable (1950–1990) and two cold periods: the Late Maunder Minimum (1675–1715) and the Dalton Minimum (1790–1830), characterized by a reduced solar activity and the occurrence of important volcanic events, respectively, as illustrated by Fig. 1. PDFs were calculated separately for the nine areas shown in Fig. 2, and with the same methodology as described in former section. Differences in the resulting PDFs for different periods (not shown here for the sake of brevity) have been tested with the Kolmogórof-Smirnov test. The results demonstrate that despite an obvious shift in the mean, the PDFs do not significantly change their structure or amplitude, and present,

CPD
9, 1803–1839, 2013

for both cold periods analysed, the same shapes depicted in Figs. 10 and 11 for each area.

A related issue is directly linked to the climate field reconstructions techniques used to reconstruct spatial fields of past temperature or precipitation based on a network of proxy data. These methods usually assume that the spatial covariance of climate anomalies remains constant (or at least can be described by a series of constant patterns like empirical orthogonal functions). We have analysed whether the spatial gradients remain constant through the simulation by calculating the evolution of the quantiles of the spatial distribution of SAT and precipitation within each sub-region of Fig. 2. The results are shown in Figs. 12 and 13 for SAT and precipitation, respectively. Shading represents the evolution of several quantiles of the spatial distribution of each variable in a different sub-area, while black line represents the median of this distribution. These quantiles have been calculated at annual basis, and separately for winter and summer. Finally, the series have been smoothed through a Hamming window of 30 time steps to facilitate the visualization.

Regarding temperature, the first aspect to note is that there are areas where the spatial gradient is specially intense (note that every graph has a different vertical scale), and thus in these areas the gain obtained from the use of the regional model is specially noticeable. The Alps for example, being the smallest area of those considered here, is the one that shows larger span, with a range between the 10 and 90 percentiles up to 8 °C in winter and 10 °C in summer. Scandinavia also presents a large heterogeneity, related with the strong North–South gradient of temperatures, although in this case the variability is larger in winter than in summer (10 °C versus 7 °C). These two areas are also those where the climate variability is more intense, with differences in the median between the coldest and the warmest periods up to 3.5 and 2.5 °C in winter for Scandinavia and the Alps, respectively. In contrast, Central Europe is one of the areas where the added value of the higher model resolution is less noticeable, with spreads between the 10 and 90 percentiles smaller than 4 and 3 °C for winter and summer, respectively, and differences in the median between the warmest and coldest period

CPD
9, 1803–1839, 2013

of about 1.4 °C in both seasons. In every area the model simulates the clear tendency toward warming in the last part of the simulation. It is preceded by a strong cold period around 1810, coincidental with an increase in the number of volcanic events and lower solar activity (Dalton Minimum), which is especially noticeable in the summer series. However, the Late Maunder Minimum (1675–1715), also a period with a reduced solar activity, is hardly noticeable in the temperature series and is rather embedded in the longer cold period generally denominated as the Little Ice Age. Regarding the question of whether the spatial heterogeneity responds to external forcing, the simulation seems to indicate that this is not the case. As in the case of the PDFs of the series around cold periods discussed above, the spatial temperature range does not seem to be modulated by the shift of the mean values.

Figure 13 depicts the same information for precipitation. Many of the conclusions derived for temperature can be extended to this variable as well. Despite variations in the mean state in different periods, the spatial gradients are very similar in different periods, retaining a rather constant spread along the simulation. However, the probability distribution of this variable presents a strong positive skewness (which can be appreciated in the asymmetry of the percentiles), which makes the tails of the distribution to behave asymmetrically in some areas where the changes in the mean value are most intense. This is apparent, for instance, in the asymmetric behaviour of the percentile trends in the distribution of winter precipitation in Scandinavia or The British Isles, where a large trend dominates the precipitation variability. The opposite behaviour can also be found when the trend is negative, like in winter precipitation in the Balkans or summer precipitation in the British Isles. Unlike SAT, there is no a clear agreement in precipitation trends in the final simulated period, when the influence of anthropogenic forcings is more intense. Winter precipitation shows a clear negative trends in areas such as Turkey, the Balkans or the Iberian Peninsula, whereas it is positive in the British Isles or Scandinavia. Similarly, summer trends are heterogeneous and show no agreement among different areas (as already illustrated by Fig. 9), which is a indication of the strong dependence of this variable on the regional features of each area. In general,

CPD
9, 1803–1839, 2013

the signal of the forcings is not apparent in these series, and even the Dalton Minimum, which can be clearly recognized in the SAT series, is not noticeable here by a coherent signal of increase or decrease of precipitation regimes. This different behaviour, weakly modulated by the external forcings, is due to the nature of this variable, strongly driven by internal variability at regional scales, as already identified by Gómez-Navarro et al. (2012) in simulations for the Iberian peninsula.

5 Summary and conclusions

In this study we have illustrated the added value of a high-resolution climate simulation over Europe for the period 1500–1990, focusing the analysis on winter and summer seasons. Using the observational dataset CRU as benchmark, the regional model is capable of generating a high-resolution realistic climatology for SAT and precipitation over most areas of Europe in the reference period 1960–1990. The configuration employed here has, however, some important biases which have to be considered when evaluating the reliability of the model. Especially noticeable is the underestimation of the amplitude of the annual cycle of temperatures, as well as the overestimation of precipitation in Northern Europe. This deficiency seems to be related to the overestimation of the zonal circulation simulated by the driving global model, a feature which is shared by other state-of-the-art GCMs.

The model also accurately reproduces the variability of the seasonal series, especially its spatial structure, with a clear North–South gradient in winter temperature and a strongly orography-modulated precipitation pattern. In general terms, the model tends to underestimate the SAT variability, although part of this difference can be attributed to the higher spatial resolution of the observational dataset, interpolated here to the model grid to perform the comparison.

We have compared the simulated and observed trends for SAT and precipitation during the 1900–1990 period. The model tends to overestimate the warming trend, especially in Northern areas in winter. In particular, the model simulates an homogeneously

CPD
9, 1803–1839, 2013

positive trend which is absent in the observations, which instead show a negative, although not statistically significant trend in the North. There may be several reasons for this difference. On the one hand, both models employed here do not include anthropogenic tropospheric aerosols as forcing. It is well known that an important anthropogenic factor has been the increase of tropospheric aerosols, whose net effect is believed to produce a net cooling. A complementary explanation for these differences can be found in the simulation of the circulation in the North Atlantic area. The model simulates a strong trend in the NAO index under anthropogenic forcing which is absent in the observations. This trend leads to a trend in the zonal flow in Northern Europe, which is consistent with the positive trends of SAT and precipitation simulated over this area and with the negative trends in winter precipitation in Southern Europe. The relationship between the observed NAO trend and the external forcing is by no means clear. Although most models in the CMIP and CMIP3 ensemble simulate a positive NAO trend in the 21st century driven by increasing greenhouse gas forcing, the long-term behaviour of the NAO in the 20th century, with negative trend until 1975, positive thereafter until 1990, and negative until present does not suggest a strong effect of the external forcing at decadal time scales. The lack of agreement between observations and simulations in the 20th century could be then just due to the uncorrelated internal variability present in both.

The added value of the regional model stands out in the calculation of the PDFs. We have compared the PDFs for SAT and precipitation during the 1900–1990 period in the GCM, the RCM and in the observations. This calculation has been performed for different areas separately in order to stress the dependence of the results on the regional features. The global model presents important biases, which the RCM is partly capable to reduce, narrowing differences with the observations. More importantly, the RCM is able to reproduce the shape of PDFs, reproducing its complex structure or even its bimodality in areas of complex topography, such as the Iberian Peninsula or the Alps. In areas with less complex orography such as Central and Eastern Europe,

CPD
9, 1803–1839, 2013

the added value of the regional models is not so clear, and the use of GCM data to compare with climate reconstructions can be a reasonable option.

We have investigated the changes of PDFs in different periods. In this respect, we have found that despite an overall shift, their statistical properties barely change along the simulations. In particular, the variance of the distributions is not significantly reduced around cold periods such as the Dalton Minimum. This seems to be in contradiction with findings in the context of climate change projections, where an increased the spread in the PDFs is also projected (Christensen. et al., 2007). However, it has to be noted that the increase of the forcings in the future projections is much stronger than the amplitude of forcing changes implemented in this paleoclimate simulation.

Acknowledgements. This work was funded by the Spanish Ministry of Science and Technology (project SPECMORE-CGL2008-06558-C02-02/CLI). J. J. Gómez-Navarro thanks the funding from the PRIME2 project (priority program INTERDYNAMIK, German Research Foundation). Thanks to Elena Bustamante and Juerg Luterbacher for the stimulating discussions.

References

Bladé, I., Fortuny, D., van Oldenborgh, G. J., and Liebmann, B.: The summer North Atlantic oscillation in CMIP3 models and related uncertainties in projected summer drying in Europe, J. Geophys. Res., 117, D16104, doi:10.1029/2012JD017816, 2012. 1815

Chen, F. and Dudhia, J.: Coupling an Advanced Land Surface-Hydrology Model with the Penn State-NCAR MM5 Modeling System, Part I: Model Implementation and Sensitivity, Mon. Weather Rev., 129, 569–585, 2001a. 1810

Chen, F. and Dudhia, J.: Coupling an Advanced Land Surface-Hydrology Model with the Penn State-NCAR MM5 Modeling System, Part II: Preliminary Model Validation, Mon. Weather Rev., 129, 587–604, 2001b. 1810

Christensen, J. H., Hewitson, B., Busuioc, A., Chen, A., Gao, X., Held, I., Jones, R., Kolli, R. K., Kwon, W.-T., Laprise, R., Rueda, V. M., Mearns, L., Menéndez, C. G., Räisänen, J., Rinke, A., Sarr, A., and Whetton, P.: Regional Climate Projections, in: Climate Change 2007: The Physical Science Basis. Contribution of Working Group I to the Fourth Assessment Report of

CPD
9, 1803–1839, 2013

the Intergovernmental Panel on Climate Change, Cambridge University Press, Cambridge, UK and New York, NY, USA, 2007. 1804, 1812, 1818, 1823

Crowley, J: Causes of Climate Change Over the Past 1000 Years, Science, 289, 270–277, doi:10.1126/science.289.5477.270, 2000. 1809

Dudhia, J.: Numerical study of convection observed during the winter monsoon experiment using a mesoscale two-dimensional model, J. Atmos. Sci., 46, 3077–3107, 1989. 1810

Dudhia, J.: A Nonhydrostatic Version of the Penn StateNCAR Mesoscale Model: Validation Tests and Simulation of an Atlantic Cyclone and Cold Front, Mon. Weather Rev., 121, 1493–1513, 1993. 1810

Fernández, J., Montávez, J. P., Saenz, J., González-Rouco, J. F., and Zorita, E.: Sensitivity of the MM5 mesoscale model to physical parameterizations for regional climate studies: Annual cycle, J. Geophys. Res.-Atmos., 112, D04101, doi:10.1029/2005JD006649, 2007. 1810

Gómez-Navarro, J. J., Montávez, J. P., Jerez, S., Jiménez-Guerrero, P., Lorente-Plazas, R., González-Rouco, J. F., and Zorita, E.: A regional climate simulation over the Iberian Peninsula for the last millennium, Clim. Past, 7, 451–472, doi:10.5194/cp-7-451-2011, 2011. 1805, 1806, 1810

Gómez-Navarro, J. J., Montávez, J. P., Jiménez-Guerrero, P., Jerez, S., Lorente-Plazas, R., González-Rouco, J. F., and Zorita, E.: Internal and external variability in regional simulations of the Iberian Peninsula climate over the last millennium, Clim. Past, 8, 25–36, doi:10.5194/cp-8-25-2012, 2012. 1806, 1815, 1821

González-Rouco, J. F., Beltrami, H., Zorita, E., and Stevens, M. B.: Borehole climatology: a discussion based on contributions from climate modeling, Clim. Past, 5, 97–127, doi:10.5194/cp-5-97-2009, 2009. 1805

Gray, L. J., Beer, J., Geller, M., Haigh, J. D., Lockwood, M., Matthes, K., Cubasch, U., Fleitmann, D., Harrison, G., Hood, L., Luterbacher, J., Meehl, G. A., Shindell, D., van Geel, B., and White, W.: Solar influence on climate, Rev. Geophys., 48, RG4001, doi:10.1029/2009RG000282, 2011. 1809

Grell, G. A.: Prognostic evaluation of assumptions used by cumulus parameterizations, Mon. Weather Rev., 121, 764–787, 1993. 1810

Grell, G. A., Dudhia, J., and Stauffer, D. R.: A description of the fifth-generation Penn State/NCAR Mesoscale Model (MM5), Tech. Rep. NCAR/TN-398+STR, National Center for Atmospheric Research, Boulder, USA, 1994. 1810

CPD
9, 1803–1839, 2013

Harris, I., Jones, P., Osborn, T., and Lister, D.: Updated high-resolution grids of monthly climatic observations – the CRU TS3.10 dataset, Int. J. Climatol., submitted, 2012. 1810, 1811
Hong, S. Y. and Pan, H. L.: Nonlocal boundary layer vertical diffusion in a medium–range forecast model, Mon. Weather Rev., 124, 2322–2339, 1996. 1810
Jerez, S., Montávez, J. P., Gómez-Navarro, J. J., Jiménez-Guerrero, P., Jiménez, J. M., and González-Rouco, J. F.: Temperature sensitivity to the land-surface model in MM5 climate simulations over the Iberian Peninsula, Meteorol. Z.,, 19, 1–12, 2010. 1810
Jerez, S., Montávez, J. P., Jiménez-Guerrero, P., Gómez-Navarro, J. J., Lorente-Plazas, R., and Zorita, E.: A multi-physics ensemble of present-day climate regional simulations over the Iberian Peninsula, Clim. Dynam., doi:10.1007/s00382-012-1539-1, in press, 2012. 1810
Kalnay, E., Kanamitsu, M., Kistler, R., Collins, W., Deaven, D., Gandin, L., Iredell, M., Saha, S., White, G., Woollen, J., Zhu, Y., Leetmaa, A., and Reynolds, R.: The NCEP/NCAR 40-Year Reanalysis Project, B. Am. Meteorol. Soc., 77, 437–470, 1996. 1813
Kanamitsu, M. and DeHann, L.: The added Value Index: A new metric to quantify the added value of regional models, J. Geophys. Res., 116, D11106, doi:10.1029/2011JD015597, 2011. 1807
Krivova, N. A., Balmaceda, L., and Solanki, S. K.: Reconstruction of solar total irradiance since 1700 from the surface magnetic flux, Astron. Astrophys., 467, 335–346, doi:10.1051/0004-6361:20066725, 2007. 1809
Legutke, S. and Voss, R.: The Hamburg atmosphere-ocean coupled circulation model ECHO-G, Tech. rep., DKRZ, Hamburg, Germany, 1999. 1808
Luterbacher, J., Dietrich, D., Xoplaki, E., Grosjean, M., and Wanner, H.: European seasonal and annual temperature variability, trends, and extremes since 1500, Science, 303, 1499–1503, 2004. 1805, 1806
Miller, R. L., Schmidt, G. A., and Shindell, D. T.: Forced annular variations in the 20th century Intergovernmental Panel on Climate Change Fourth Assessment Report models, J. Geophys. Res., 111, 1–17, doi:10.1029/2005JD006323, 2006. 1815
Mlawer, E. J., Taubman, S. J., Brown, P. D., Iacono, M. J., and Clough, S. A.: Radiative transfer for inhomogeneous atmospheres: RRTM, a validated correlated- model for the longwave, J. Geophys. Res., 102, 16663–16682, 1997. 1810
Murphy, J.: An evaluation of statistical and dynamical techniques for downscaling local climate, J. Climate, 12, 2256–2284, 1999. 1807

CPD
9, 1803–1839, 2013

Osborn, T. J. and Hulme, M.: Development of a Relationship between Station and Grid-Box Rainday Frequencies for Climate Model Evaluation, J. Climate, 10, 1885–1908, doi:10.1175/1520-0442(1997)010<1885:DOARBS>2.0.CO;2, 1997. 1812

Pauling, A., Luterbacher, J., Casty, C., and Wanner, H.: Five hundred years of gridded high-resolution precipitation reconstructions over Europe and the connection to large-scale circulation , Clim. Dynam., 26, 387–405, doi:10.1007/s00382-005-0090-8, 2006. 1805, 1806

Prömmel, K., Geyer, B., Jones, J. M., and Widmann, M.: Evaluation of the skill and added value of a reanalysis-driven regional simulation for Alpine temperature, Int. J. Climatol., 773, 760–773, doi:10.1002/joc.1916, 2009. 1807

Schimanke, S., Meier, H. E. M., Kjellström, E., Strandberg, G., and Hordoir, R.: The climate in the Baltic Sea region during the last millennium simulated with a regional climate model, Clim. Past, 8, 1419–1433, doi:10.5194/cp-8-1419-2012, 2012. 1806

Shapiro, A. I., Schmutz, W., Rozanov, E., Schoell, M., Haberreiter, M., Shapiro, A. V., and Nyeki, S.: A new approach to the long-term reconstruction of the solar irradiance leads to large historical solar forcing, Astron. Astrophys., 529, A67, doi:10.1051/0004-6361/201016173, 2011. 1809

Zorita, E., Von Storch, H., Gonzalez-Rouco, J. F., Cubasch, U., Luterbacher, J., Legutke, S., Fischer-Bruns, I., and Schlese, U.: Climate evolution in the last five centuries simulated by an atmosphere–ocean model: global temperatures, the North Atlantic Oscillation and the Late Maunder Minimum, Meteorol. Z., 13, 271–289, doi:10.1127/0941-2948/2004/0013-0271, 2004. 1809

Zorita, E., González-Rouco, J. F., von Storch, H., Montávez, J. P., and Valero, F.: Natural and anthropogenic modes of surface temperature variations in the last thousand years, Geophys. Res. Lett., 32, 755–762, 2005. 1809

Zorita, E., Moberg, A., Leijonhufvud, L., Wilson, R., Brázdil, R., Dobrovolny, P., Luterbacher, J., Böhm, R., Pfister, C., Riemann, D., Glaser, R., Söderberg, J., and Gonzalez-Rouco, F.: European temperature records of the past five centuries based on documentary information compared to climate simulations, Climatic Change, 101, 143–168, doi:10.1007/s10584-010-9824-7, 2010. 1805

CPD
9, 1803–1839, 2013

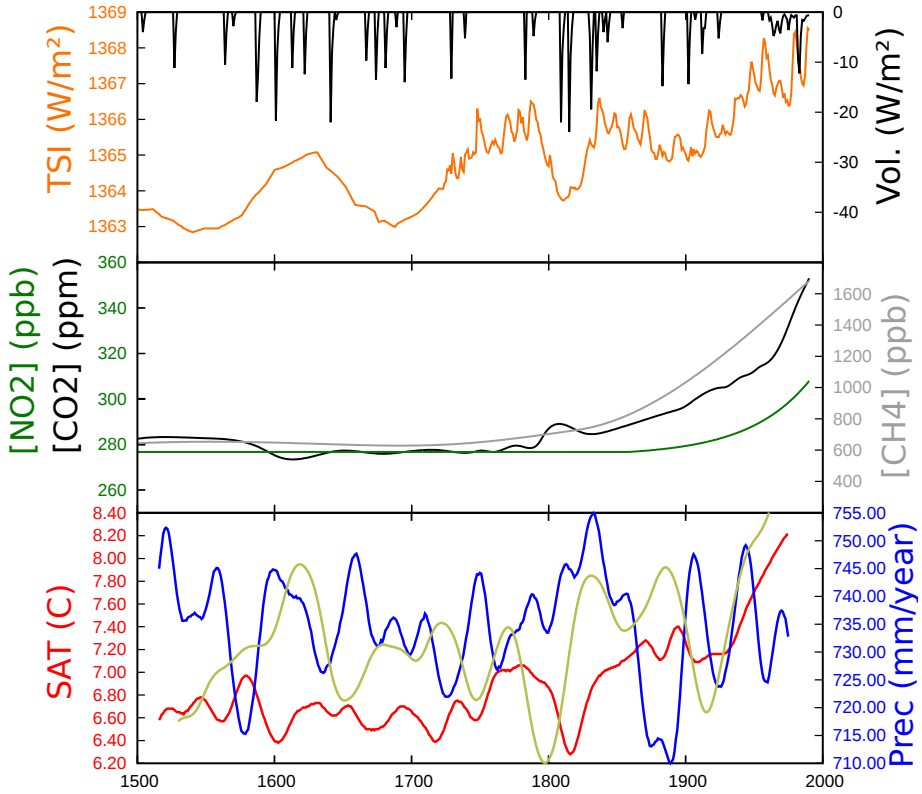

Fig. 1. Forcings implemented in the simulation and evolution of spatial-averaged SAT (red) and precipitation (blue) over the whole domain in the regional simulation. The (dimensionless) NAO index is also presented in dark yellow. The original annual series in the bottom panel have been high-frequency filtered using a Hamming window.

CPD
9, 1803–1839, 2013

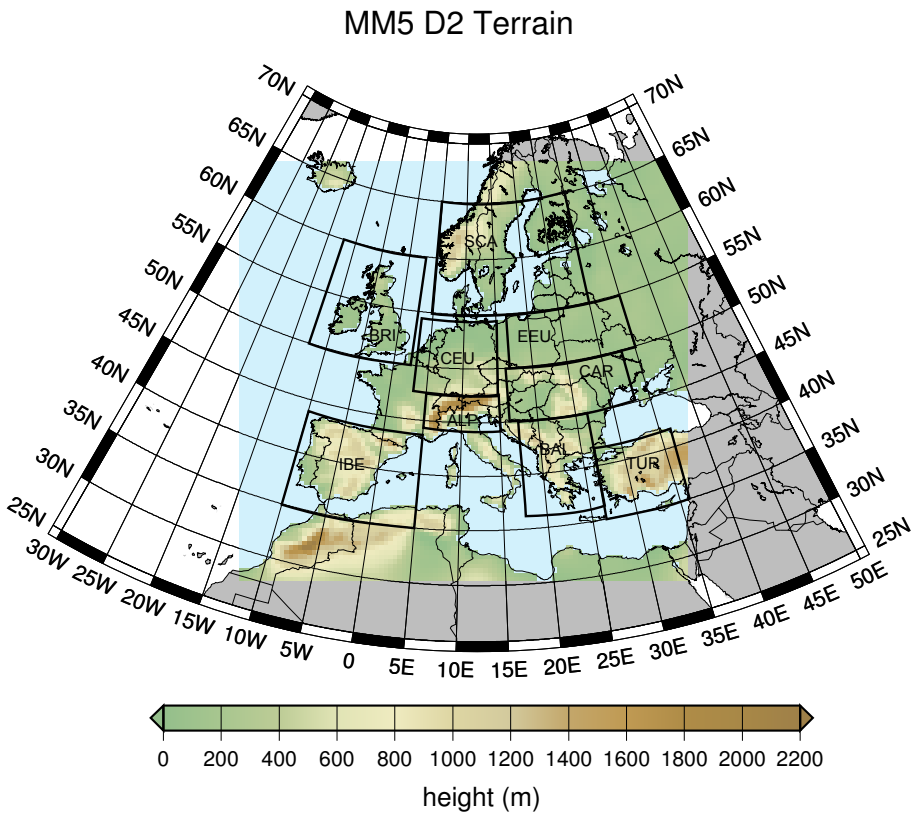

Fig. 2. Topography implemented in the inner domain of the MM5 simulation, with a spatial resolution of 45 km. The mother domain covers a larger area with 135 km of resolution (not shown). The figure illustrates the 9 subregions, selected according to geographical considerations, used for more detailed analysis hereafter: IBE, Iberian Peninsula; BRI, British Isles; CEU, Central Europe; EEU, Eastern Europe; SCA, Scandinavian Peninsula and Baltic Sea; CAR, Carpathian Region; BAL, Balkan Peninsula; ALP, Alps; TUR, Turkey.

CPD
9, 1803–1839, 2013


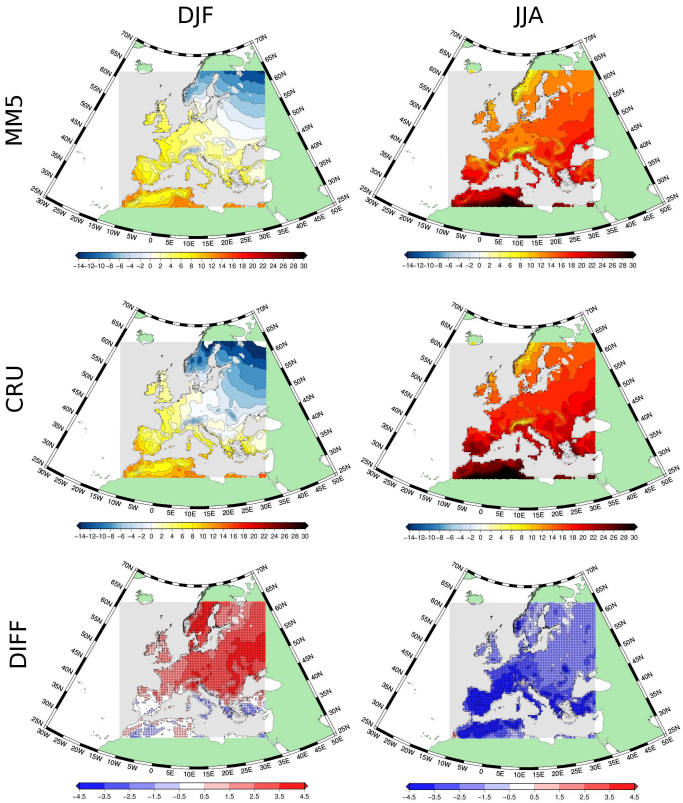

Fig. 3. SAT averaged (in ˚C) for the 1960–1990 period in winter (left panels) and summer (right panels) in the coupled model MM5-ECHO-G (top panels), CRU (middle panels) and difference between both (bottom panels). To perform the calculations, the observational dataset has been spatially interpolated to the MM5 grid, and only non ocean grid-cells have been considered. The significance of the differences have been tested through a two-tailed *t* test at the 95 % confidence level and it is indicated with small black circles in the figure.

CPD
9, 1803–1839, 2013

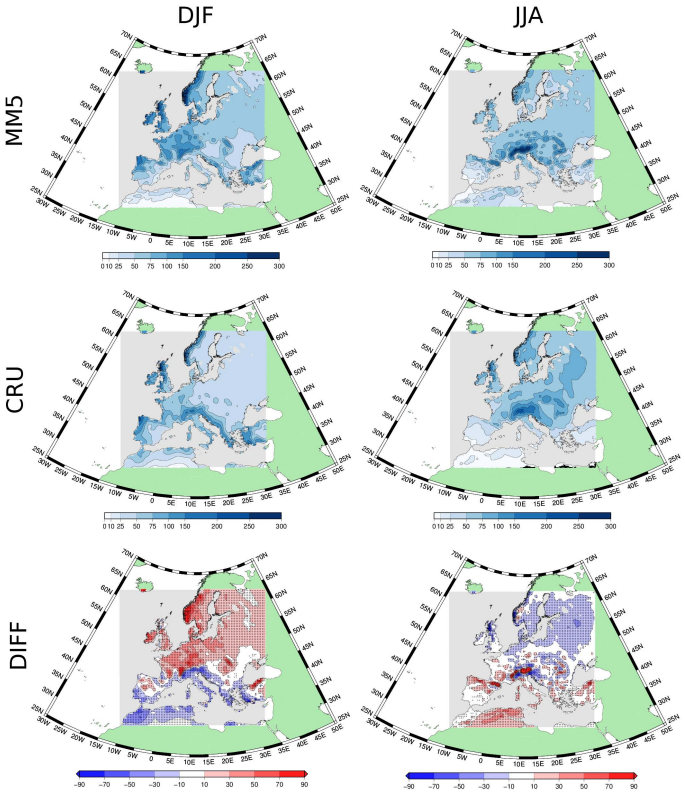

Fig. 4. Precipitation averaged (in mm month^{-1}) for the 1960–1990 period in winter (left panels) and summer (right panels) in the coupled model MM5-ECHO-G (top panels), CRU (middle panels) and difference (in percentage) between both (bottom panels). To perform the calculations, the observational dataset has been spatially interpolated to the MM5 grid, and only non ocean grid-cells have been considered. The significance of the differences have been tested through a two-tailed *t* test at the 95 % confidence level and it is indicated with small black circles in the figure.

CPD
9, 1803–1839, 2013

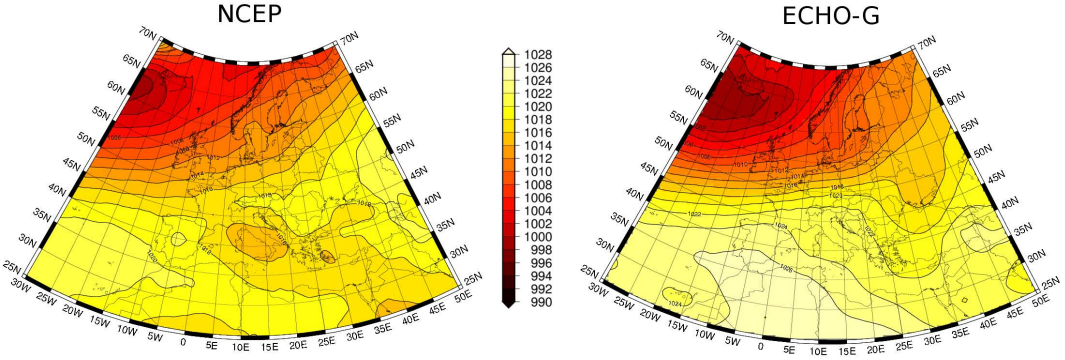

Fig. 5. MSLP in winter in the reference period in the NCEP reanalysis (left panel) and simulated by ECHO-G (right panel). The units are hPa.

CPD
9, 1803–1839, 2013

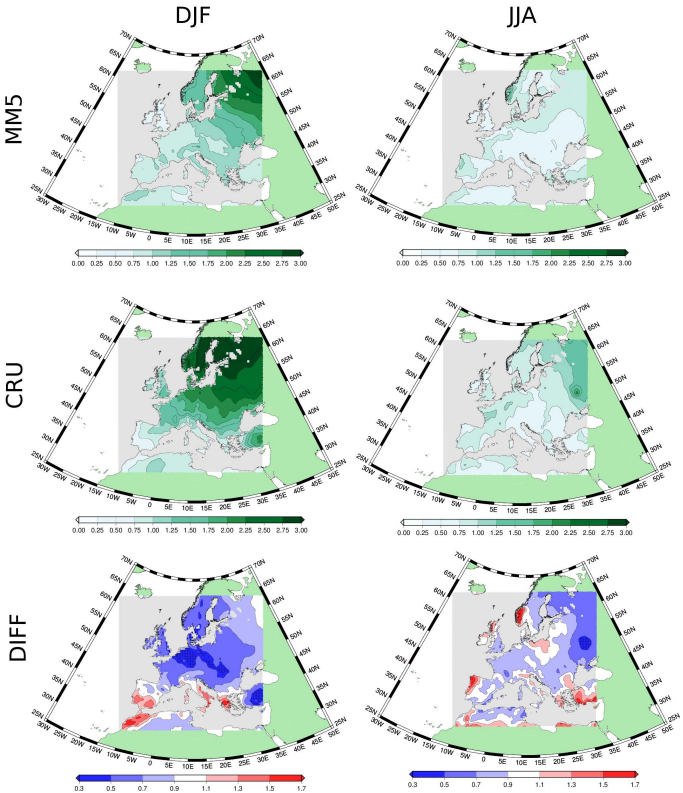

Fig. 6. Standard deviation of seasonal SAT series (in ˚C) in the reference period for winter (left panels) and summer (right panels) in the coupled model MM5-ECHO-G (top panels), CRU (middle panels) and ratio between both (bottom panels). To perform the calculations, the observational dataset has been spatially interpolated to the MM5 grid, and only non ocean grid-cells have been considered. The significance of the ratio have been tested through a two-tailed *F* test at the 95 % confidence level and it is indicated with small black circles in the figure.

CPD
9, 1803–1839, 2013

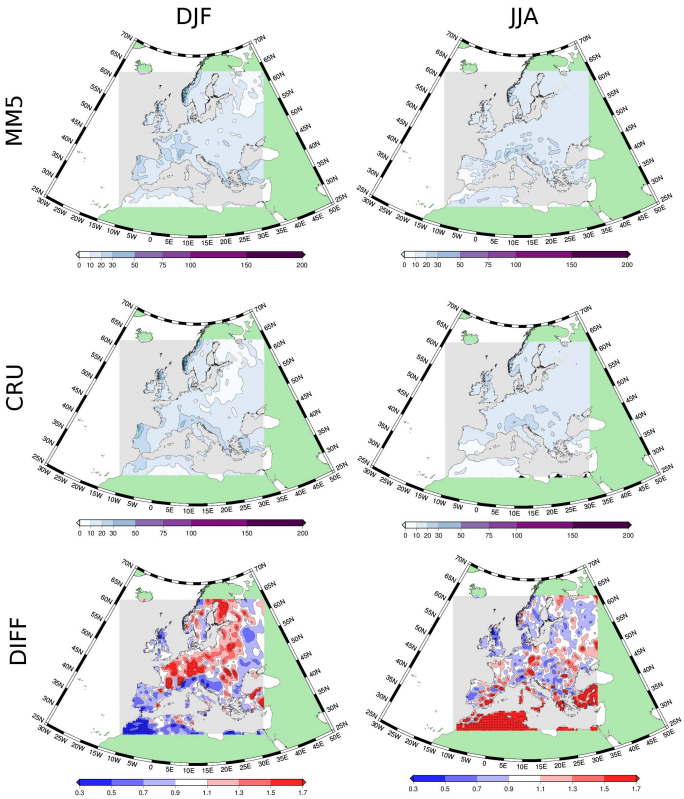

Fig. 7. Standard deviation of seasonal precipitation series (in mm month^{-1}) in the reference period for winter (left panels) and summer (right panels) in the coupled model MM5-ECHO-G (top panels), CRU (middle panels) and ratio between both (bottom panels). To perform the calculations, the observational dataset has been spatially interpolated to the MM5 grid, and only non ocean grid-cells have been considered. The significance of the differences have been tested through a two-tailed *T* test at the 95 % confidence level and it is indicated with small black circles in the figure.

CPD
9, 1803–1839, 2013

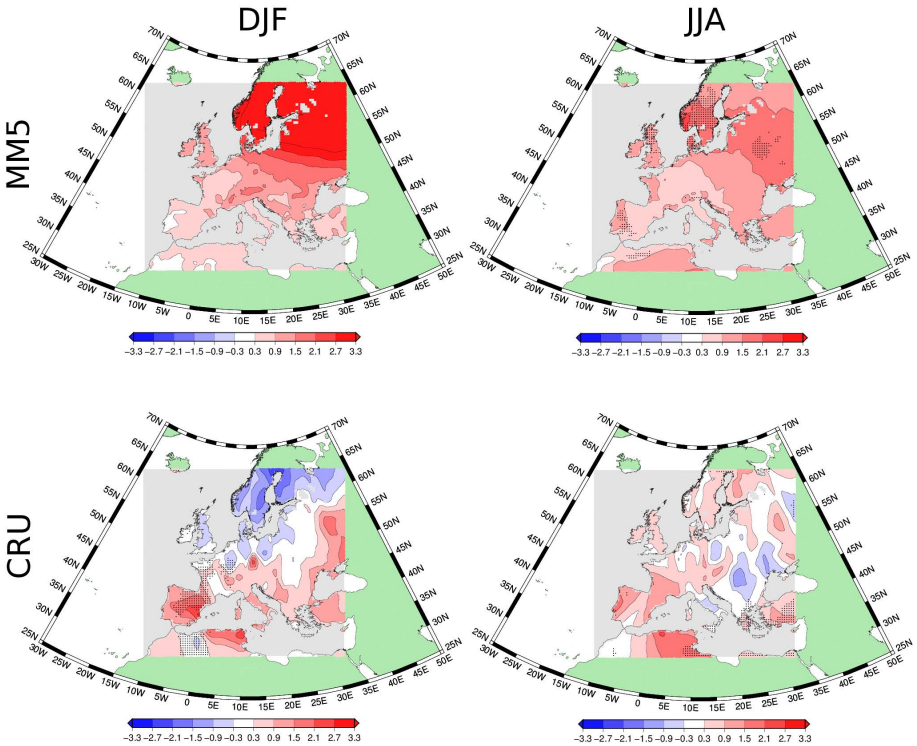

Fig. 8. Trends (in K century^{-1}) in the seasonal SAT series in the 1900–1990 period for winter (left panels) and summer (right panels) in the coupled model MM5-ECHO-G (top panels) and CRU (bottom panels). To perform the calculations, the observational dataset has been spatially interpolated to the MM5 grid, and only non ocean grid-cells have been considered. The significance of the trends have been tested through the Mann–Kendall test assuming that series are uncorrelated, and it is indicated with small black circles in the figure.

CPD
9, 1803–1839, 2013

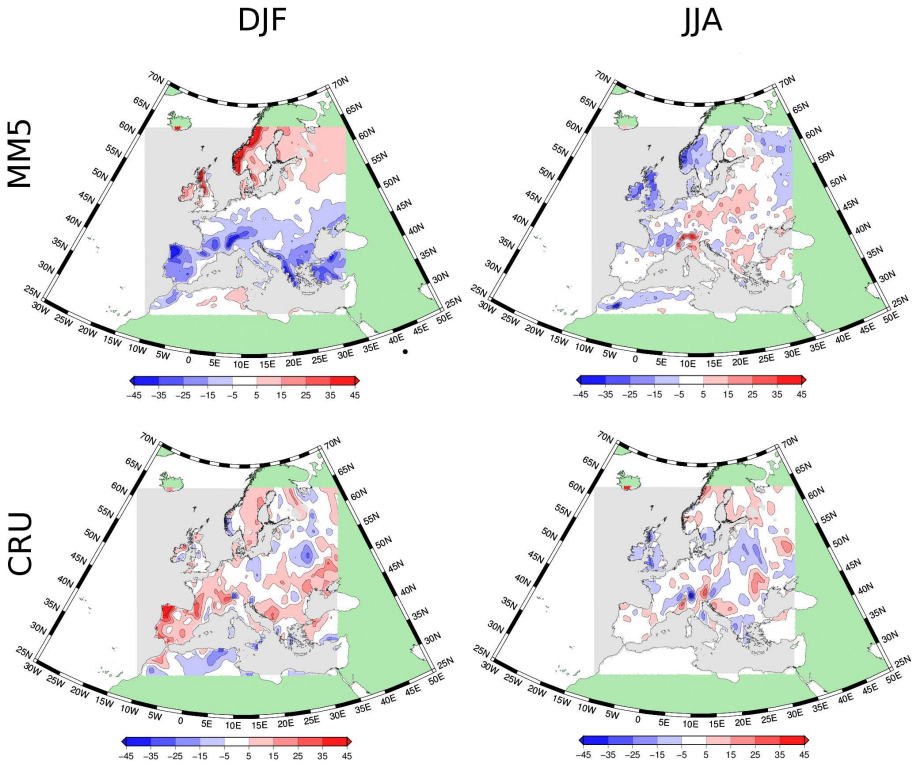

Fig. 9. Trends (in mm month^{-1} century^{-1}) in the seasonal precipitation series in the 1900–1990 period for winter (left panels) and summer (right panels) in the coupled model MM5-ECHO-G (top panels) and CRU (bottom panels). To perform the calculations, the observational dataset has been spatially interpolated to the MM5 grid, and only non ocean grid-cells have been considered. The significance of the trends have been tested through the Mann–Kendall test assuming that series are uncorrelated, and it is indicated with small black circles in the figure.

CPD
9, 1803–1839, 2013

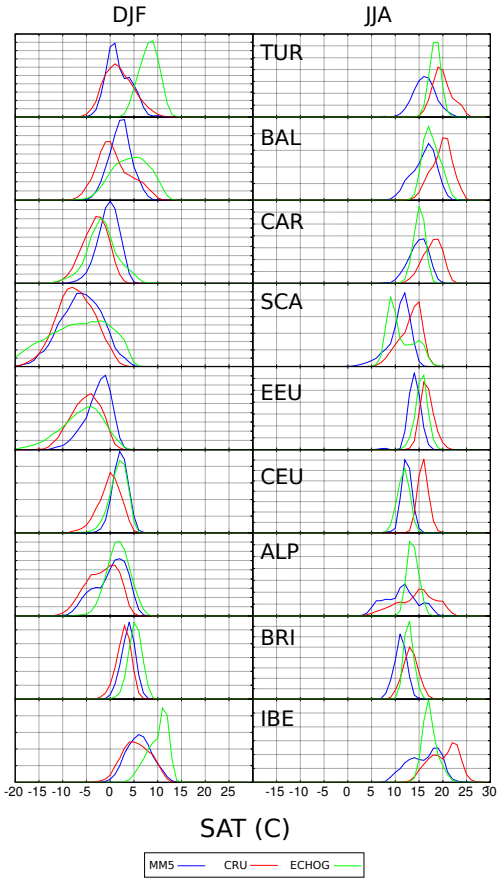

Fig. 10. PDF of seasonal series of SAT in nine sub-areas of Europe shown in Fig. 2. The results for winter (left panel) and summer (right panel) are presented for MM5, ECHO-G and the CRU dataset. The horizontal axis shows the units of SAT in Celsius degree, while the vertical indicates relative frequency and the corresponding values have been omitted.

CPD
9, 1803–1839, 2013

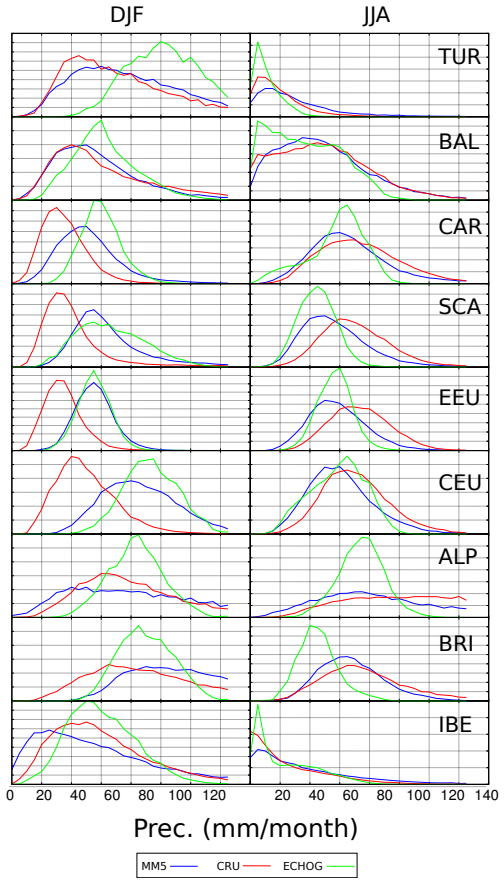

Fig. 11. PDF of seasonal series of precipitation in nine sub-areas of Europe shown in Fig. 2. The results for winter (left panel) and summer (right panel) are presented for MM5, ECHO-G and the CRU dataset. The horizontal axis shows the units of precipitation in mm/month, while the vertical indicates relative frequency and the corresponding values have been omitted.

CPD
9, 1803–1839, 2013

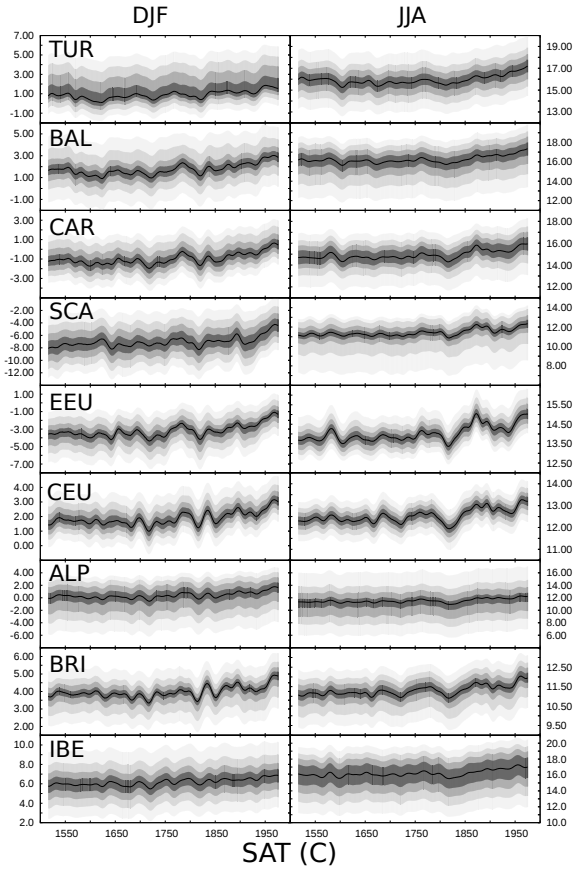

Fig. 12. Temporal series of SAT quantiles in the nine areas considered in Fig. 2. The filled curve encompasses the 10 and 90 percentiles of the SAT field in each time step, while the solid line represents the median. The series have been smoothed through a Hamming window of 30 timesteps to emphasise the low-frequency variability.

CPD
9, 1803–1839, 2013




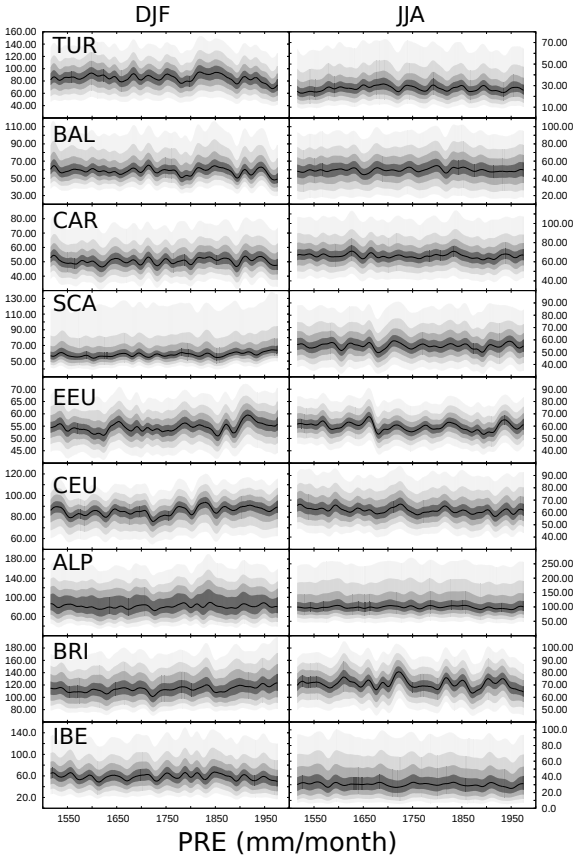

Fig. 13. Temporal series of precipitation quantiles in the nine areas considered in Fig. 2. The filled curve encompasses the 10 and 90 percentiles of the precipitation field in each time step, while the solid line represents the median. The series have been smoothed through a Hamming window of 30 timesteps to emphasise the low-frequency variability.

CPD
9, 1803–1839, 2013